Editors' Suggestion | Featured in Physics

Fano Combs in the Directional Mie Scattering of a Water Droplet

Javier Tello Marmolejo,[1,*] Adriana Canales,[2] Dag Hanstorp,[1] and Ricardo Méndez-Fragoso[3]
[1]Department of Physics, University of Gothenburg, SE-412 96 Gothenburg, Sweden
[2]Department of Physics, Chalmers University of Technology, SE-412 96 Gothenburg, Sweden
[3]Facultad de Ciencias, Universidad Nacional Autónoma de México, Alcaldía Coyoacán, C.P. 04510 Ciudad Universitaria, Ciudad de México, México

(Received 28 April 2022; revised 22 June 2022; accepted 13 December 2022; published 24 January 2023)

When light scatters off a sphere, it produces a rich Mie spectrum full of overlapping resonances. Single resonances can be explained with a quantum analogy and result in Fano profiles. However, the full spectrum is so complex that recognizable patterns have not been found, and is only understood by comparing to numerical simulations. Here we show the directional Mie spectrum of evaporating water droplets arranged in consecutive Fano Combs. We then fully explain it by expanding the quantum analogy. This turns the droplet into an "optical atom" with angular momentum, tunneling, and excited states.

DOI: 10.1103/PhysRevLett.130.043804

Introduction.—The scattering of an electromagnetic wave by a dielectric sphere was first calculated by Gustav Mie in 1908 [1]. Despite the simplicity of a sphere and a plane wave, this problem leads to a rich spectrum of radius-dependent resonances called Mie resonances. For particles significantly larger than the wavelength, some of these resonances cause the light to internally reflect around the circumference of the sphere. This creates a surface effect called whispering gallery modes that appears every time the circumference is a multiple of the wavelength inside the material [2–5].

Mie resonances can have quality factors several orders of magnitude higher than Fabry-Perot resonators [2], making them ideal as sensors [5,6] or as laser cavities [7]. They are also suitable for obtaining self-hybridized polaritons to potentially change the material properties of a sample [8,9].

In 1977, Arthur Ashkin observed Mie resonances in the scattering force of an optically levitated solid microparticle [10]. For solid spheres, the radius is fixed, and Mie resonances can be found by varying the trapping wavelength of the laser, but the spectrum's range is limited by the tunable range of the laser.

Varying the size is analogous to scanning the wavelength. Thus, much wider, radius-dependent Mie spectra can be achieved using evaporating droplets. However, stable optical trapping can be complicated because the weight and optical forces vary considerably as the droplet shrinks, causing it to drift in the trap or be lost. One solution is to use slowly evaporating liquids such as glycerol [11] or salt-water solution [12]. Droplets can also be trapped in electric quadrupole traps and probed by light-emitting diodes [13] or lasers [14].

Here we built a counterpropagating optical trap to observe the Mie resonances of evaporating water droplets at a fixed laser frequency. We used the optical levitation technique first demonstrated by Ashkin *et al.* [15] and later applied in various fields ranging from sensor development [16] to juggling with light [17]. Our trap keeps rapidly shrinking droplets stable and provides consistent electromagnetic excitation. Thus we obtain a Mie spectrum with a smooth, continuous, dependence on the size of the scatterer.

Numerical methods are commonly employed to calculate Mie spectra [18] and are compared to the experimental results [11,12,19–21]. However, although the simulations reproduce the experimental spectra, they do not reveal an intuitive understanding of the complicated structure. When the vector components of the electric field decouple owing to the symmetry, as with a sphere, the solution depends on a scalar wave equation. This is identical to the Schrödinger equation with an appropriate potential. Thus, individual Mie resonances can be understood through a quantum mechanical analogy [3,4,22,23]. However, Mie spectra are a result of many overlapping resonances, and only understanding a single resonance falls short. Here, we expand this analogy to several series of resonances at once to explain the full Mie spectrum we observe.

Another connection to quantum physics is Fano profiles, first observed in the scattering of electrons [24]. The Fano nature of Mie resonances in subwavelength particles was predicted [25] and observed [26] when focusing on a singled out angular direction and polarization. To observe Mie Fano resonances at wide angles, special geometries have been engineered such as ring-disc cavities [27] or multilayer nanoshells [28]. However, although the full Mie spectrum is predicted to be composed of a series of Fano

resonances [29–32], these experiments only show a small number of Fano resonances at a time.

Here, we show the directional Mie scattering of evaporating water droplets. By focusing on a specific direction and polarization, we managed to isolate only the transverse magnetic modes. This leads to over 100 evolving Fano resonances organized in consecutive *Mie Fano combs*. Inside each comb, they transform smoothly from wide Lorentzians to sharp Fano profiles. This appears naturally in a simple water sphere, in contrast to previous predictions of Mie Fano combs in purposefully engineered plasmonic particles [33]. We then provide a theoretical understanding by expanding the previous quantum-mechanical analogy making it possible to fully explain the now simplified *directional Mie spectrum* and its *Fano comb* structure.

This analogy converts the experiment into an "optical atom." Here, photons are trapped instead of electrons, and the attractive potential is a result of the droplet's refractive index instead of the Coulomb force. The system shows atomic properties as quantized angular momentum, tunneling, and excited states. This creates a link between optics and atomic physics since the spherical potential well of the droplets is similar to that of atoms [34] and negative ions [35], where similar Fano resonances can be observed.

Experimental setup.—We built a counterpropagating optical trap (Fig. 1) where we levitated water droplets in air and measured the scattering intensity of the droplets as they evaporated. It is capable of trapping droplets from radii of $\simeq 6$ μm down to full evaporation with a constant position, ensuring a consistent electromagnetic excitation throughout the process.

We divided a 532.0 nm, continuous-wave laser beam into two vertically polarized arms and focused them into the same spot from opposite directions inside the trapping chamber. We focused each arm using a 100 mm and a 65 mm lens, resulting in beam waists of 7.5 ± 0.8 μm and 4.9 ± 0.5 μm, respectively. These were chosen to be comparable to the size of the investigated droplets. Since the optical forces change significantly as the droplet shrinks, careful balancing between the intensities and alignment of both arms was needed to keep the position of the evaporating droplet stable.

We used an ultrasonic nebulizer (MY-520A) to dispense a cloud of water droplets into the trapping chamber. Droplets randomly fell into the optical trap and merged into the largest droplet the trap could hold. After the cloud settled, the remaining droplet quickly evaporated ($\simeq 10$ s).

Mie Fano comb structure.—Mie resonances result from two linearly independent modes inside the sphere, the spherical transverse electric (TE) and transverse magnetic (TM) modes. We selected only the TM modes by focusing on the I_θ polarization component of the scattering perpendicular to the tapping laser (see inset of Fig. 1 and Supplemental Material [36]).

This selection results in a simplified *directional Mie spectrum* with a periodic structure, shown in Fig. 2(a). The lower x axis shows the measured radius of the droplet (see the Supplemental Material [36]), and the upper x axis the size parameter $x = ka$.

As opposed to nondirectional Mie spectra [11,12,19,20], the entire spectrum can be understood as a series of separate resonances where at most two overlap, and each can be clearly identified.

We observe three distinct, overlapping combs inside of which the resonances are equidistant. The leftmost comb does not overlap with a new one to its left, meaning that this is the first comb with the lowest order whispering gallery modes. These modes cannot exist for smaller spheres since the wavelength becomes comparable to the circumference and light cannot *coil* around the surface of the sphere.

Each comb is composed of distinct Fano resonances that evolve from being symmetric (Lorentz form) to the asymmetric shape of a Fano resonance. Figure 2(b) shows

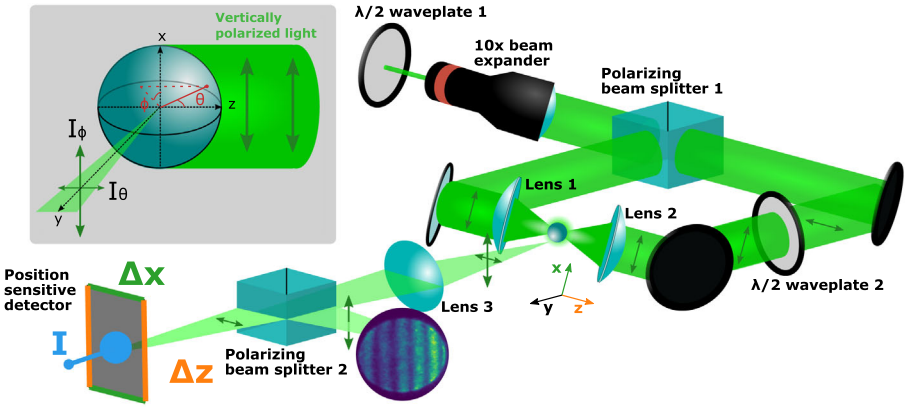

FIG. 1. Counterpropagating trap used to record *directional Mie* spectra of evaporating water droplets. The green arrows mark the laser's polarization. The I_θ polarization was focused onto a position sensitive detector to measure the scattering intensity. I_ϕ was projected onto a transparent screen to observe the interference pattern and calculate the droplet's radius.

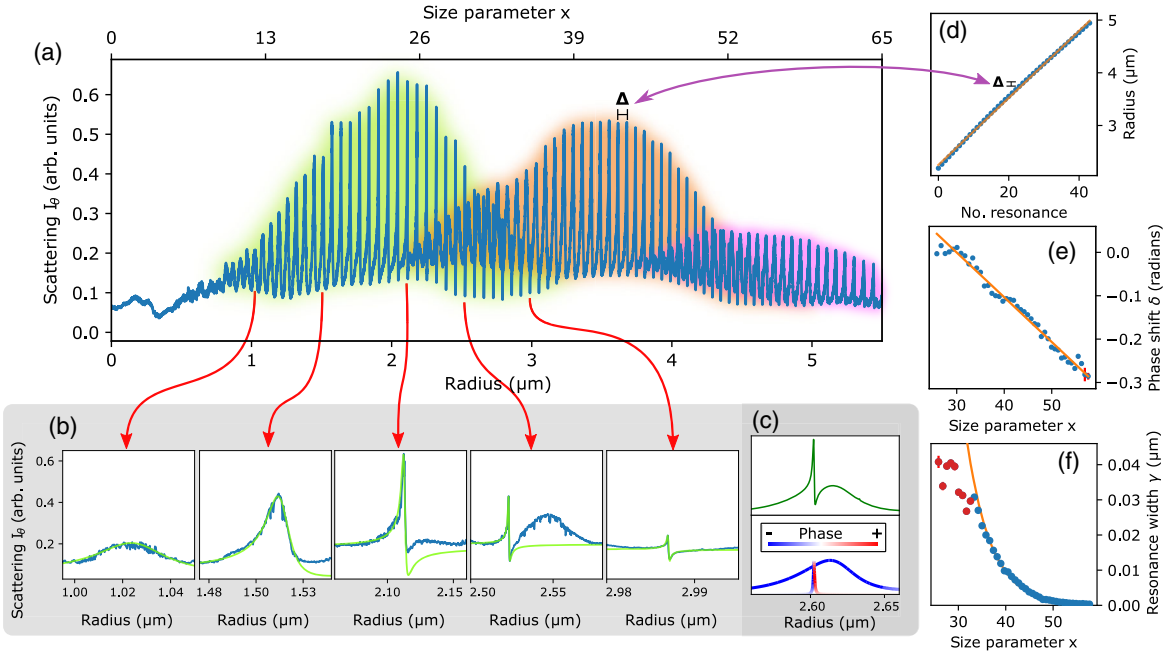

FIG. 2. *Fano Comb* structure of the directional Mie scattering. (a) Directional scattering intensity I_θ as the droplet shrinks. Highlighted are the first three *combs* composed of equidistant, evolving Fano resonances. (b) Evolution of the resonances from Lorenztians to Fano through five selected segments of the first comb. A fit to the Fano equation, Eq. (1), is shown in green. (c) Mie simulation showing the interference between two resonances at the intersection of two combs (below) producing a sharp Fano profile (above). (d)–(f) Fano parameters obtained from fits of Eq. (1) on the second comb. The separation between resonances inside a comb is constant (d), the phase shift δ starts at zero and decreases linearly until 0.3π (e), and the resonance width γ decreases exponentially (f).

selected resonances fitted using Fano's equation including a noninteracting component of the background [29]

$$\sigma(\Omega) = D^2\left[\frac{(q+\Omega)^2}{1+\Omega^2}\eta + (1-\eta)\right], \tag{1}$$

where $q = \cot(\delta)$ is the Fano parameter, δ is the phase shift with the continuum, $\eta \in [0,1]$ is an interaction coefficient, and $D^2 = 4\sin^2(\delta)$. Usually, Ω is a function of the energy with $\Omega = 2(E - E_0)/\Gamma$, where Γ is the resonance width and E_0 the energy of the resonance. Here, we replaced the energy in Ω with the radius of the sphere since size a and energy $\propto k$ are interchangeable with respect to the size parameter, $x = ka$.

The Fano profile is produced by the flip of the phase before and after a resonance as shown in the Mie mode simulation of Fig. 2(c). For a sphere, the scattering cross section results in Lorentzian resonances, and the Fano profiles are a directional effect (see the Supplemental Material [36]).

Figure 2(d) shows the constant separation between resonances, where we plotted the center of each resonance in the second comb obtained from the fit of Eq. (1). The slope is $\Delta = 63.6 \pm 2.3$ nm resulting in resonances occurring with every change in circumference of $2\pi\Delta = 399 \pm 14$ nm. In other words, the light coils around inside the droplet, and constructive interference occurs every time the circumference is a multiple of the wavelength inside the material, $\lambda/n = 399.1$ nm.

The fitting of each individual resonance confirms predictions of Mie scattering being composed of a series of Fano resonances [29–32]. Additionally, it unites the wide and sharp resonances commonly observed in Mie scattering spectra as the same phenomenon through a smooth transition of the parameters in Eq. (1). Figures 2(e) and 2(f) show the evolution of the phase shift δ and resonance width γ inside the second comb. The phase shift decreases linearly from 0 to 0.3π while the resonance width decreases exponentially. At $\gamma = 0.03$ μm the free spectral range becomes comparable to the resonance width, and γ cannot be measured accurately (red dots).

The optical atom.—Common practice would be to perform a simulation of Mie scattering and compare to the spectrum in Fig. 2(a). However, simulations do not provide an intuitive understanding of the spectrum, and the relation to the Fano equation is usually shown analytically [30,31]. Instead, we explain the full spectrum of resonances through an extension of the well-known quantum mechanical analogy [3,4] previously used to explain one single resonance and its phase shift [43].

From Maxwell's equations, we know that for a nonmagnetic, uncharged sphere with radius a, the electric field must follow the equation

$$\nabla \times (\nabla \times \boldsymbol{E}) - k^2 n^2(r)\boldsymbol{E} = 0, \tag{2}$$

where $\mathbf{E}$ is the electric field, $k = 2\pi/\lambda$ the wave number, and $n(r)$ the refractive index. In this case, n is a step function with $n(r < a) = n_{\text{water}}$ and $n(r > a) = n_{\text{air}}$.

Following the procedure outlined by Johnson [3], the radial dependence of the electric field $S_\ell(r)$ must satisfy the differential equation

$$\frac{d^2S_\ell(r)}{dr^2} + \left[k^2n^2(r) - \frac{\ell(\ell+1)}{r^2}\right]S_\ell(r) = 0. \quad (3)$$

This applies for both the TE and TM modes as long as we consider the refractive index to be a step function, i.e., $dn(r)/dr = 0$.

If we define the energy as $E = k^2$ and choose a square potential well $V(r) = -k^2[n^2(r) - 1]$, then the radial, time-independent Schrödinger equation with a central potential and with $\hbar/2\mu = 1$ becomes

$$\frac{d^2\Psi(r)}{dr^2} + \left[k^2[n^2(r)-1] - \frac{\ell(\ell+1)}{r^2}\right]\Psi(r) = -E\Psi(r), \quad (4)$$

which is identical to Eq. (3). The effective potential becomes

$$V_{\text{eff}}(r) = \frac{\ell(\ell+1)}{r^2} - k^2[n^2(r) - 1]. \quad (5)$$

Solving for the electric field is mathematically analogous to solving the Schrödinger equation [Eq. (4)]. Thus, we can use the interpretation of resonances from quantum mechanics to understand the spectrum we observe.

The effective potential is a spherical well potential. It results from the sum of an attractive square well and the centrifugal barrier. A bound energy level in this potential can be understood as the light trapped inside the droplet, continuously reflecting on the inner surface. The rotation around the circumference gives the light quantized angular momentum ℓ.

Figure 3(a) shows four *wedged potential wells* (blue) and their calculated energy levels for spheres of different radii. An energy level represents the "energy of the laser," k^2, needed to produce a Mie resonance inside a sphere of that size. Note that this is only in terms of the quantum potential and is not related to the usual laser energy $h\nu$.

These energy levels are numbered by the radial number N and are known in atomic physics as ground state ($N = 1$) and *excited states* ($N = 2, 3, \ldots$). The radii at which energy levels match the "energy of the laser" and create a resonance are shown in Fig. 3(b) (see the Supplemental Material [36]). It shows the three distinct combs, first in green, second in orange, and third in purple.

Figure 3(c) shows the scattering for three selected resonances. The resonances from the first comb (green) are related to the first energy level inside the wedge, a^1_ℓ. When the well becomes wide enough, an additional energy level appears, a^2_ℓ, and the second comb begins (orange). In this way, each specific mode is defined through the double index a^N_ℓ (a for TM) and b^N_ℓ (b for TE) where N is the radial

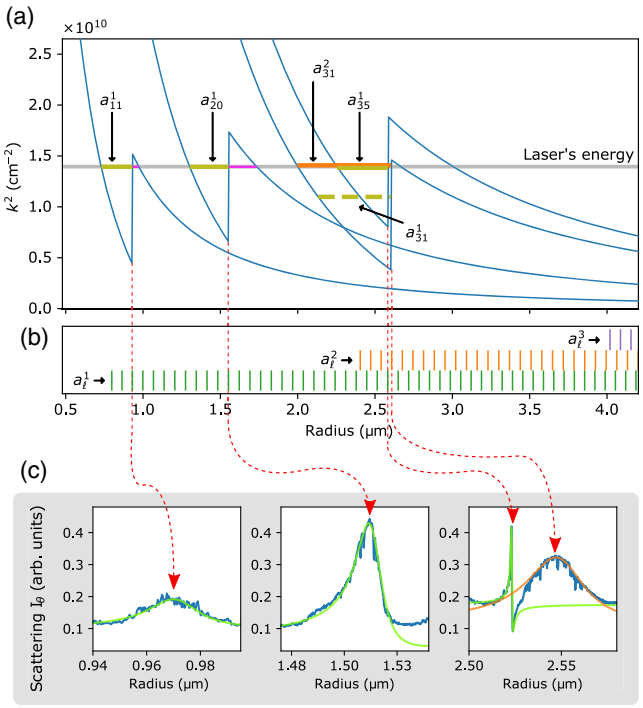

FIG. 3. The shape of the wedged well potential defines the profile of the resonance. (a) $V_{\text{eff}}(r)$ for $\ell = 11$, 20, 31, and 35. The energy levels inside the wedge are plotted with green (first comb) and orange (second comb). The magenta lines mark the potential barriers for $\ell = 11$ and 20. The energy level a^1_{31} is dashed to mark that it does not resonate with the laser. See the Supplemental Material [36] for a video of the energy levels in a growing sphere. (b) All the calculated energy levels up to 4.5 μm, showing the basis for the comb structure. (c) The directional scattering at three selected size ranges of the droplet (blue) and a fit using Eq. (1).

quantum number [8,12] arising from the roots of the boundary conditions. Notice that the equations giving the resonances do not depend on the value of "m" due to the angular degeneracy in Eq. (2) and the spherical geometry of the scattering target.

The first resonance, a^1_{11}, has a narrow barrier (magenta line), resulting in a wide, Lorentzian resonance. For the next resonant levels, a^1_{20} and a^1_{35}, the barrier becomes wider and results in narrower resonances.

As a wave meets the potential barrier, one part reflects, and another tunnels through, resonates, and leaks out. The phase shift between the reflected and resonant waves leads to constructive and destructive interference, producing the asymmetric Fano profiles shown in Fig. 3(c). A similar phase shift occurs in resonances from atomic potentials with similar shapes [44].

As the barrier widens tunneling becomes harder, and the resonances begin to narrow and shrink. Then, new resonances start to appear resulting from the second energy level, exemplified by a^2_{31} in Fig. 3(a). It is again trapped behind a narrow barrier, producing a Lorentzian resonance

and starting the second comb [rightmost panel of Fig. 3(c) in orange]. Both sets of resonances (a_l^1 and a_l^2) overlap until the barriers of the first energy levels eventually become so wide that the first comb dies off, as shown in Fig. 2(a). The process repeats all over again for each set of higher energy levels, resulting in the sequence of combs. This is best understood through the video shown in the Supplemental Material [36].

Inside a comb, the barrier width is approximately proportional to the size parameter (see the Supplemental Material [36]). Thus, the evolution of γ and δ [Figs. 2(d) and 2(e)] can be explained through the barrier width. Large barriers make it harder to tunnel, reducing γ exponentially. This agrees with the exponential increase of the Q factor shown previously [23]. Similarly, δ increases linearly as the evanescent wave travels through wider barriers and gains a larger phase for smaller shifts away from the resonance.

Conclusion.—We have revealed a *directional Mie spectrum* with a simpler structure than previous Mie scattering spectra. We achieved this by stably trapping evaporating water droplets, isolating the TM modes, and measuring their directional Mie scattering.

The periodic appearance of the Mie resonances can be used as a ruler to measure the evaporation rates of droplets with nanometric precision. Additionally, the spectrum is highly dependent on the refractive index and its spatial distribution. It could be used to measure the concentration of biological or chemical substances on the surface of evaporating droplets. We estimate a sensitivity to a real refractive index of $\simeq 3 \times 10^{-4}$ and in absorption of $\simeq 1 \times 10^{-3}$. Since the choice of wavelength is free, maximizing the difference in n between water and the substance could yield a sensitivity of up to 1 part per 10^3.

We confirmed that Mie resonances are composed of a series of Fano resonances, found that they are arranged in consecutive combs, and explained all of these characteristics through a quantum mechanical analogy. This makes it possible to fully explain Mie spectra without the need for numerical simulations.

Finally, the spectrum results from a simple, finite spherical potential well. This is just one level of complexity above the classical square potential well taught in all quantum mechanics courses. Thus, this experiment becomes an "optical atom" where light is trapped inside a droplet in the same way as an electron would be trapped in a spherical well model of an atomic potential.

The supporting data for this Letter as well as the video of the interference fringes of the evaporating droplet are openly available from [45].

We thank Mats Rostedt for his help with I. T. Financial support from the Swedish Research Council (2019-02376) is acknowledged. R. M.-F. acknowledges financial support from The Wenner-Gren Foundations and the Grants No. DGAPA-PASPA, No. PAPIIT-IN-112721, and No. PAPIME-PE-103021. D. H. coordinated the project. J. T. M. built the experimental system, conducted the experiments, and analyzed the data. All authors contributed to the theoretical explanation. R. M.-F. performed the numerical calculations. J. T. M. and R. M.-F. wrote the draft of the manuscript. All authors contributed to the final version of the manuscript.

*javier.marmolejo@physics.gu.se

[1] G. Mie, Beiträge zur optik trüber medien, speziell kolloidaler metallösungen, Ann. Phys. (Leipzig) **330**, 377 (1908).
[2] G. C. Righini, Y. Dumeige, P. Féron, M. Ferrari, G. Nunzi Conti, D. Ristic, and S. Soria, Whispering gallery mode microresonators: Fundamentals and applications, Riv. Nuovo Cimento **34**, 435 (2011).
[3] B. R. Johnson, Theory of morphology-dependent resonances: Shape resonances and width formulas, J. Opt. Soc. Am. A **10**, 343 (1993).
[4] L. G. Guimarães and H. M. Nussenzveig, Theory of Mie resonances and ripple fluctuations, Opt. Commun. **89**, 363 (1992).
[5] M. R. Foreman, J. D. Swaim, and F. Vollmer, Whispering gallery mode sensors, Adv. Opt. Photonics **7**, 168 (2015).
[6] W. Kim, Ŝ. Kaya Özdemir, J. Zhu, L. He, and L. Yang, Demonstration of mode splitting in an optical microcavity in aqueous environment, Appl. Phys. Lett. **97**, 8 (2010).
[7] A. Kiraz, A. Sennaroglu, S. Doğanay, M. A. Dündar, A. Kurt, H. Kalaycioğlu, and A. L. Demirel, Lasing from single, stationary, dye-doped glycerol/water microdroplets located on a superhydrophobic surface, Opt. Commun. **276**, 145 (2007).
[8] C. E. Platts, M. A. Kaliteevski, S. Brand, R. A. Abram, I. V. Iorsh, and A. V. Kavokin, Whispering-gallery exciton polaritons in submicron spheres, Phys. Rev. B **79**, 245322 (2009).
[9] A. Canales, D. G. Baranov, T. J. Antosiewicz, and T. Shegai, Abundance of cavity-free polaritonic states in resonant materials and nanostructures, Chem. Phys. **154**, 1 (2021).
[10] A. Ashkin and J. M. Dziedzic, Observation of Resonances in the Radiation Pressure on Dielectric Spheres, Phys. Rev. Lett. **38**, 1351 (1977).
[11] T. C. Preston, B. J. Mason, J. P. Reid, D. Luckhaus, and R. Signorell, Size-dependent position of a single aerosol droplet in a bessel beam trap, J. Opt. **16**, 025702 (2014).
[12] A. D. Ward, M. Zhang, and O. Hunt, Broadband mie scattering from optically levitated aerosol droplets using a white led, Opt. Express **16**, 16390 (2008).
[13] M. B. Hart, V. Sivaprakasam, J. D. Eversole, L. J. Johnson, and J. Czege, Optical measurements from single levitated particles using a linear electrodynamic quadrupole trap, Appl. Opt. **54**, F174 (2015).
[14] J. Archer, M. Kolwas, D. Jakubczyk, G. Derkachov, M. Woźniak, and K. Kolwas, Evolution of radius and light scattering properties of single drying microdroplets of colloidal suspension, J. Quantum Spectrosc. Radiat. Transfer. **202**, 168 (2017).
[15] A. Ashkin and J. M. Dziedzic, Optical levitation by radiation pressure, Appl. Phys. Lett. **19**, 283 (1971).

[16] C. Gonzalez-Ballestero, M. Aspelmeyer, L. Novotny, R. Quidant, and O. Romero-Isart, Levitodynamics: Levitation and control of microscopic objects in vacuum, Science **374**, eabg3027 (2021).
[17] A. J. Bae, D. Hanstorp, and K. Chang, Juggling with Light, Phys. Rev. Lett. **122**, 043902 (2019).
[18] P. Lalanne, W. Yan, K. Vynck, C. Sauvan, and J. Hugonin, Light interaction with photonic and plasmonic resonances, Laser Photonics Rev. **12**, 1700113 (2018).
[19] P. Chýlek, J. T. Kiehl, and M. K. W. Ko, Optical levitation and partial-wave resonances, Phys. Rev. A **18**, 2229 (1978).
[20] R. E. Willoughby, M. I. Cotterell, H. Lin, A. J. Orr-Ewing, and J. P. Reid, Measurements of the imaginary component of the refractive index of weakly absorbing single aerosol particles, J. Phys. Chem. A **121**, 5700 (2017).
[21] C. L. Price, A. Bain, B. J. Wallace, T. C. Preston, and J. F. Davies, Simultaneous retrieval of the size and refractive index of suspended droplets in a linear quadrupole electrodynamic balance, J. Phys. Chem. A **124**, 1811 (2020).
[22] M. A. M. Marte and S. Stenholm, Paraxial light and atom optics: The optical Schrödinger equation and beyond, Phys. Rev. A **56**, 2940 (1997).
[23] T. J. Kippenberg, Nonlinear optics in ultra-high-Q whispering-gallery optical microcavities, Ph.D. thesis, California Institute of Technology, Pasadena, CA, 2004.
[24] U. Fano, Effects of configuration interaction on intensities and phase shifts, Phys. Rev. **124**, 1866 (1961).
[25] M. I. Tribelsky, S. Flach, A. E. Miroshnichenko, A. V. Gorbach, and Y. S. Kivshar, Light Scattering by a Finite Obstacle and Fano Resonances, Phys. Rev. Lett. **100**, 043903 (2008).
[26] M. I. Tribelsky, J.-M. Geffrin, A. Litman, C. Eyraud, and F. Moreno, Directional Fano resonances in light scattering by a high refractive index dielectric sphere, Phys. Rev. B **94**, 121110(R) (2016).
[27] Y. Sonnefraud, N. Verellen, H. Sobhani, G. A. E. Vandenbosch, V. V. Moshchalkov, P. V. Dorpe, P. Nordlander, and S. A. Maier, Experimental realization of subradiant, superradiant, and Fano resonances in ring/disk plasmonic nanocavities, ACS Nano **4**, 1664 (2010).
[28] Z. Hao, Y. Gao, Z. Huang, X. Liang, and Y. Liu, Plasmonic fano switches in Au-SiO_2-Au multilayer nanoshells with broken core, Mater. Res. Express **4**, 095006 (2017).
[29] M. F. Limonov, M. V. Rybin, A. N. Poddubny, and Y. S. Kivshar, Fano resonances in photonics, Nat. Photonics **11**, 543 (2017).
[30] M. V. Rybin, K. B. Samusev, I. S. Sinev, G. Semouchkin, E. Semouchkina, Y. S. Kivshar, and M. F. Limonov, Mie scattering as a cascade of Fano resonances, Opt. Express **21**, 30107 (2013).
[31] M. I. Tribelsky and A. E. Miroshnichenko, Giant in-particle field concentration and Fano resonances at light scattering by high-refractive-index particles, Phys. Rev. A **93**, 053837 (2016).
[32] X. Kong and G. Xiao, Fano resonance in high-permittivity dielectric spheres, J. Opt. Soc. Am. A **33**, 707 (2016).
[33] F. Monticone, C. Argyropoulos, and A. Alù, Multilayered Plasmonic Covers for Comblike Scattering Response and Optical Tagging, Phys. Rev. Lett. **110**, 113901 (2013).
[34] R. P. Madden and K. Codling, New Autoionizing Atomic Energy Levels in He, Ne, and Ar, Phys. Rev. Lett. **10**, 516 (1963).
[35] I. Yu. Kiyan, U. Berzinsh, J. Sandström, D. Hanstorp, and D. J. Pegg, Spectrum of Doubly Excited States in the K^- Ion, Phys. Rev. Lett. **84**, 5979 (2000).
[36] See Supplemental Material at http://link.aps.org/supplemental/10.1103/PhysRevLett.130.043804 for details about (1) isolating the TM modes, (2) the size measurement of evaporating droplets, (3) the total scattering cross section of a sphere, (4) the calculations of the energy levels, (5) a video showing the potential wells, V_ℓ, and their energy levels for a water sphere with increasing radius, and (6) a plot of barrier width as a function of size parameter. It includes Refs. [37–42].
[37] M. I. Tribelsky, Phenomenological approach to light scattering by small particles and directional Fano's resonances, Europhys. Lett. **104**, 34002 (2013).
[38] M. I. Mishchenko, A. A. Lacis, and L. D. Travis, *Scattering, Absorption, and Emission of Light by Small Particles* (Cambridge University Press, Cambridge, England, 2002).
[39] C. F. Bohren and D. R. Huffman, *Absorption and Scattering of Light by Small Particles* (Wiley, New York, 1983).
[40] J. T. Marmolejo, M. Urquiza-González, O. Isaksson, A. Johansson, R. Méndez-Fragoso, and D. Hanstorp, Visualizing the electron's quantization with a ruler, Sci. Rep. **11**, 10703 (2021).
[41] T. R. Lettieri, W. D. Jenkins, and D. A. Swyt, Sizing of individual optically levitated evaporating droplets by measurement of resonances in the polarization ratio, Appl. Opt. **20**, 2799 (1981).
[42] F. W. J. Olver, D. W. Lozier, R. F. Boisvert, and C. W. Clark, *The NIST Handbook of Mathematical Functions* (Cambridge University Press, Cambridge, England, 2010).
[43] P. Kennedy, N. Dombey, and R. L. Hall, Phase shifts and resonances in the Dirac equation, Int. J. Mod. Phys. A **19**, 3557 (2004).
[44] H. Friedrich, *Theoretical Atomic Physics* (Springer-Verlag, Berlin Heidelberg, 1990), Sec. 1.4.3, pp. 37–39.
[45] J. T. Marmolejo, A. Canales, D. Hanstorp, and R. Méndez-Fragoso, Data for "Fano Combs in the Directional Mie Scattering of a Water Droplet" (2022), 10.6084/m9.figshare.17032712.